Long-term Trends in Borehole Strainmeter and Tiltmeter Data

E. Roeloffs, USGS, July 2005

1.Introduction

On the lab bench, a borehole strainmeter is an instrument with "flat response down to DC". That is, its electronic output maintains a constant ratio to applied deformation as frequency of the deformation declines to zero. After the strainmeter is installed in the borehole, however, long-term strain occurs as the borehole equilibrates to the pressure relief of drilling, and to subsequent filling with instruments and expansive grout. These strains are typically 10's of microstrain per year. They must be "removed" from the strainmeter data before shorter-term tectonic signals with amplitudes as small as a few nanostrain can be discerned. This process also removes any possible information about absolute long-term strain rates. High-pass convolution filtering may be unsatisfactory because of gaps in the data and/or step-like tectonic strains due to earthquakes or slow earthquakes.

While the first-order strain due to borehole deformation or grout curing can easily be separated from the data, variations with periods of days to months or even years typically remain. Some of these variations may be tectonic, but many of them appear to be of other origin. The long-period limit to which borehole strainmeter data may be useful needs to be estimated for each individual instrument. The situation is similar for borehole tiltmeters.

The first objective of this section is to familiarize you with the types of trends that have been recorded using existing strainmeters and tiltmeters. The next objective is to present methods for removing these trends from the data. The third objective of this section is to present examples of variations in borehole strain data at periods of months to years and to discuss ways of distinguishing tectonic from non-tectonic variations.

2. Examples of long-term records of continuous deformation data

2.1 Dilatometers

Figure 1 shows long-term records from the dilatometers at Parkfield, California. All except Vineyard Canyon (vc01) show contractional strain, consistent with a tendency of the borehole and grout to contract around the instrument. For a dilatometer, an extensional long-term strain, such as observed at Vineyard Canyon, may be an indication that the instrument is poorly coupled to the earth, a possibility that will be further discussed later.

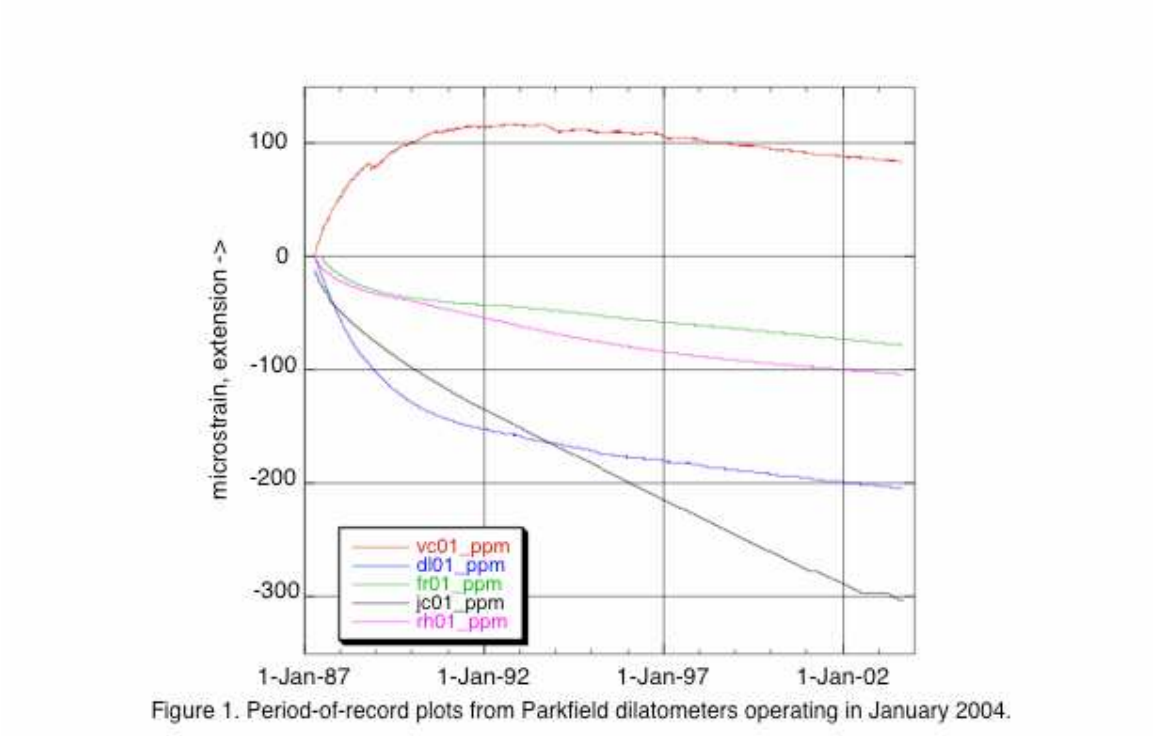

Figure 1. Graph showing long-term records from the dilatometers at Parkfield, California.

Figure 2 shows long-term records from dilatometers at Long Valley, California. The record from Devil's Postpile (popa) is especially interesting. The first instrument in this borehole failed in 1996; the cement was drilled out of the borehole and a new dilatometer was installed just above the old one. The duration of the "installation transient" is only a

few months - suggesting that ,at least at this site, relaxation of the rocks around the borehole is the mechanism causing trends that last for many years. The Devil's Postpile strainmeter also exhibits a large seasonal strain signal that will be discussed in the section on fluid pressure coupling.

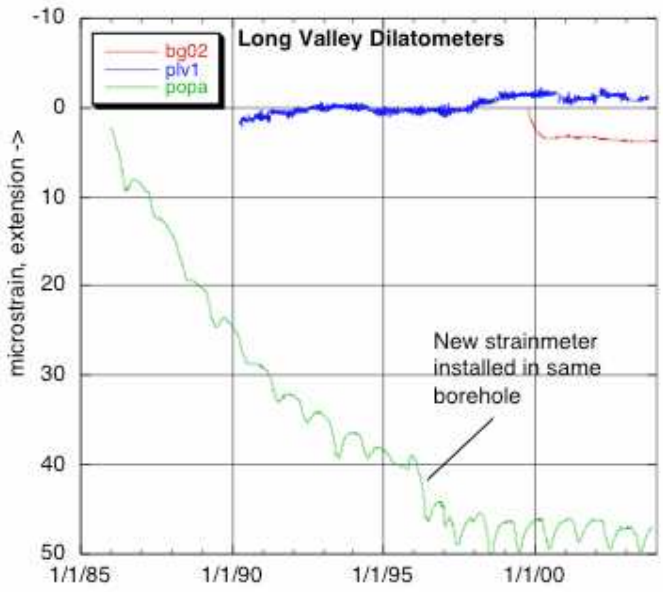

Figure 2. Graph showing long-term records from the three of the dilatometers at Long Valley caldera, California.

Also shown in Figure 2 is the data record from the Phillips (plv1) dilatometer. This instrument exhibits very little long-term strain, and what there is, is extensional. Actually, the data from plv1 exhibit very little earth tidal signal, and are instead dominated with variations that resemble atmospheric pressure. Plv1 may be an example of a "decoupled" strainmeter, to be discussed in the section on hydrologic coupling.

2.2 GTSM's

Figures 3 thru 6 show long-term records from the Frolich, Eades, Coldbrook, and San Juan Bautista GTSM's operating in California. The data shown are the "raw linearized" outputs from the individual gauges. The Frolich and San Juan Bautista instruments exhibit long-term extension on at least one gauge. This does not necessarily represent a problem, as an initially circular borehole is expected to deform into an

approximately elliptical shape, so that one axis may lengthen. Slow earthquakes and coseismic steps are prominent in the record from the San Juan Bautista (sjb) GTSM. The Coldbrook record, and to a lesser extent, the Frolich record, illustrate that the long-term trend in the data is not necessarily a smooth exponential-type function.

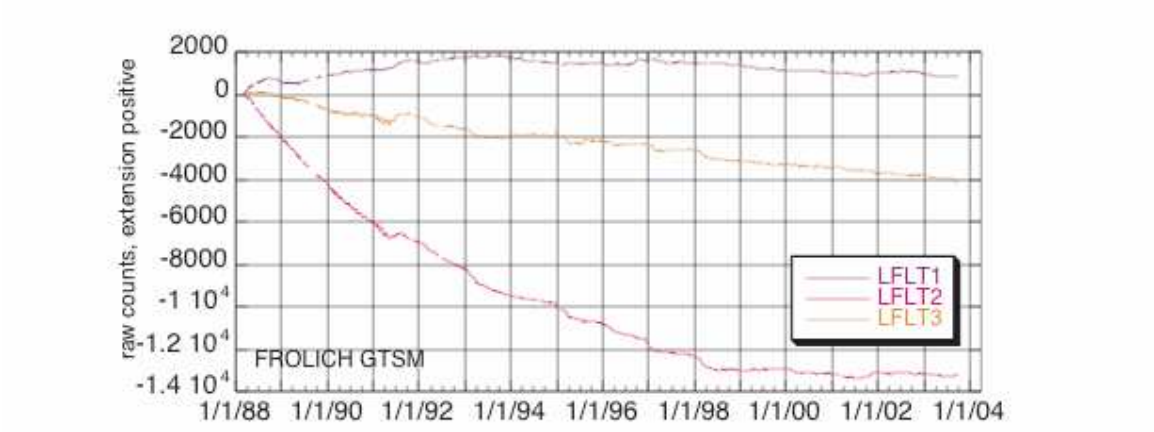

Figure 3. Long term data from the Frolich GTSM near Parkfield, California. Data shown are "raw linearized"data.

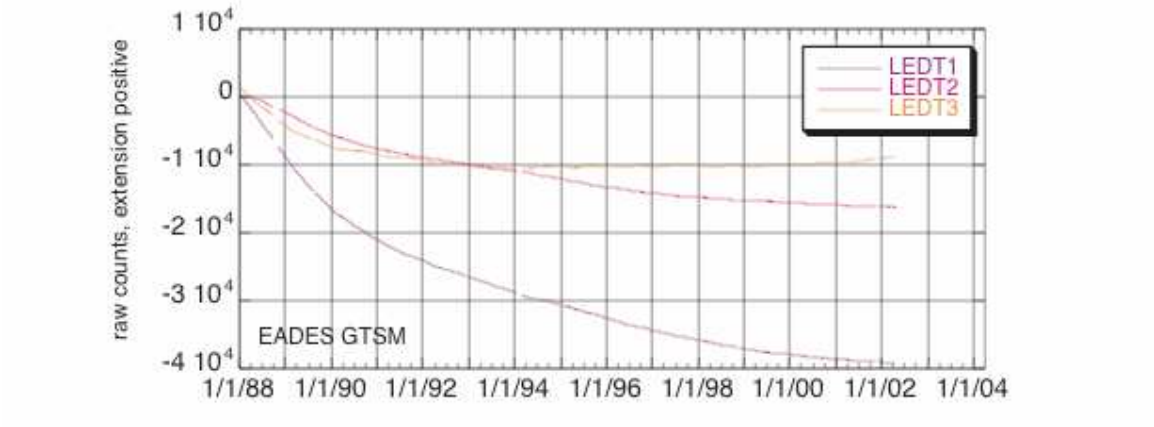

Figure 4. Long term data from the Eades GTSM near Parkfield, California. Data shown are "raw linearized"data.

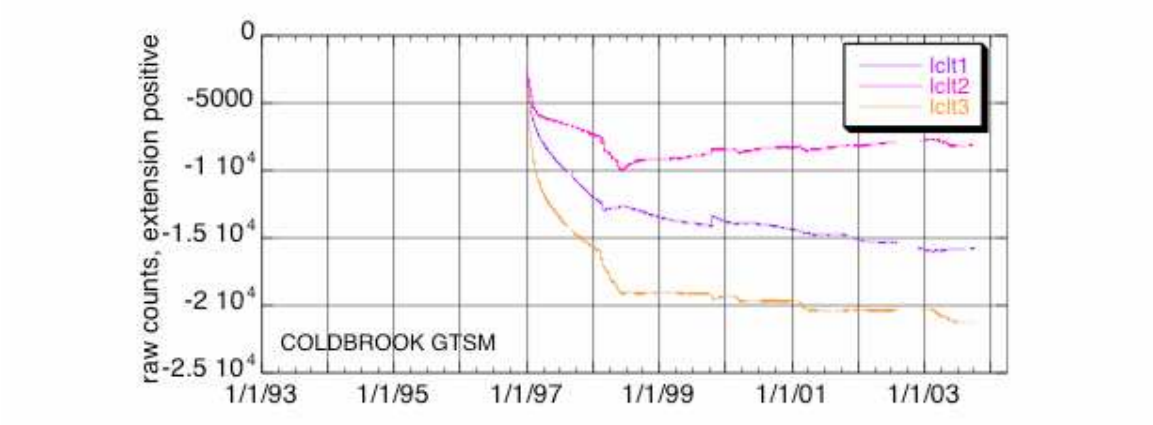

Figure 5. Long term data from the Coldbrook GTSM in southern California. Data shown are "raw linearized"data.

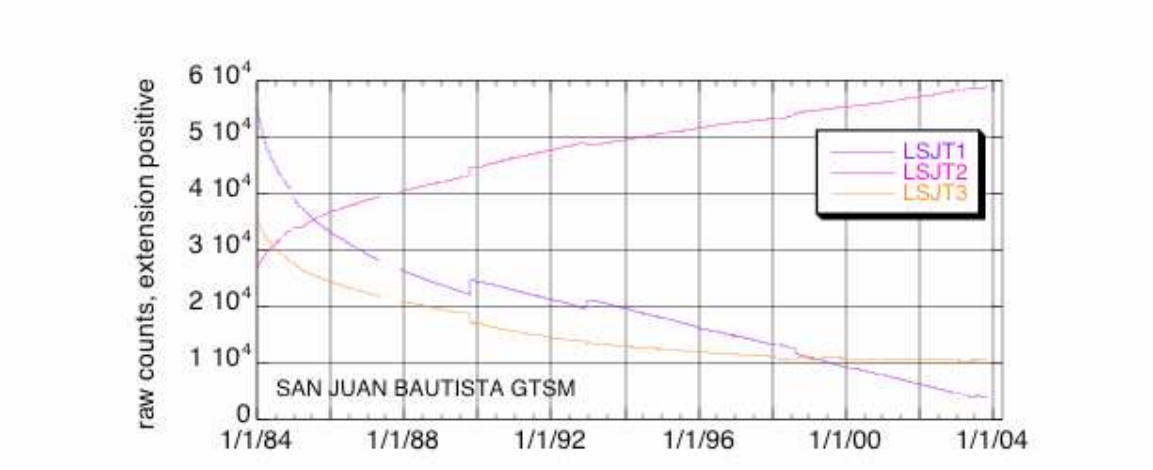

Figure 6. Long term data from the San Juan Bautista, California, GTSM. Data shown are "raw linearized"data.

2.3 Borehole tiltmeters

Hodgkinson (2004) reviewed the performance of USGS-installed borehole tiltmeters. Figure 7 shows long-term records of mini-PBO tiltmeter data from the San Francisco Bay area, after editing and correction of offsets. These tiltmeters Pinnacle 5000 bubble tiltmeters, are cemented 44-59 m below the ground surface. Many of the borehole tiltmeters also exhibit installation transients and the long-term tilt rates (often 2 microradians per month) generally far exceed those expected based on the strike-slip tectonics of the area.

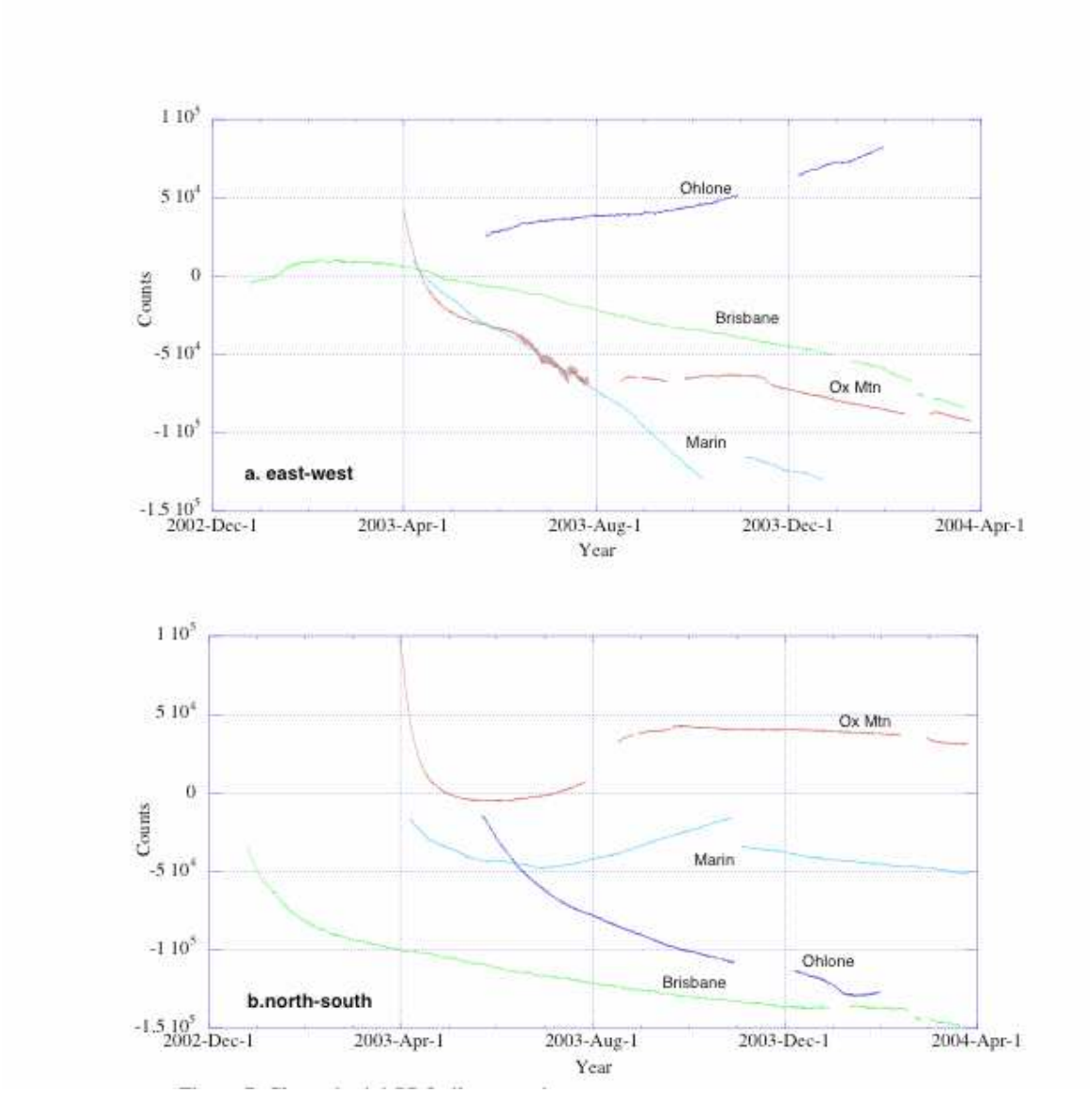

Figure 7. Long term data from the mini-PBO borehole tiltmeters in the San Francisco Bay area. From Hodgkinson, 2004.

3. Removing long-term trends from continuous deformation data

There are four basic techniques for removing long-term trends from data records: 1) high-pass filtering, 2) fitting and subtracting a parametric function, 3) subtracting a smooth non-parametric curve that approximates the data, and 4) separating the trend from other features in the data based on their distinct statistical properties. Methods (2) and (3) are illustrated here. Baytap-G provides an example of method (4).

3.1 Fitting of parametric functions to the data

The long-term trends in borehole strainmeter data are often monotonic, with slopes that decrease with time; they are frequently referred to as "exponential" trends. Functions typically used in fitting long-term borehole strain trends are of the form A+ Bt+C1 exp(D1t) + C2 exp (D2t). The fit can be carried out using daily data values and a nonlinear regression routine (for example, Marquardt's method, implemented in the Numerical Recipes routine mrqmin).

For some instruments, this method yields a reasonably good fit, and better fits can be obtained by including steps, quadratic polynomials, etc., in the data. Data gaps don't usually pose a problem. However, potential problems are that a) the data do not always appear to have a simple functional form, and b) the coefficients determined by curve-fitting change as the length of the data record included in the fit lengthens. If a fit to data collected for a fixed period of time is used to correct data for subsequent times, then it is common for the residual to contain apparent strain-rate changes; therefore projecting future values based on fits to any parametric function should be avoided.

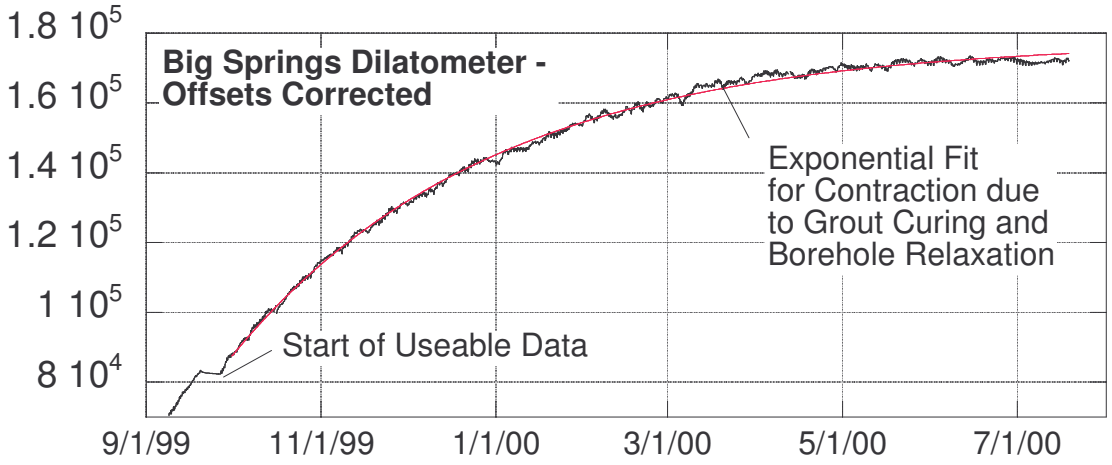

Figure 8. Data from the Big Springs dilatometer at Long Valley caldera, California. Y-axis units are arbitrary.

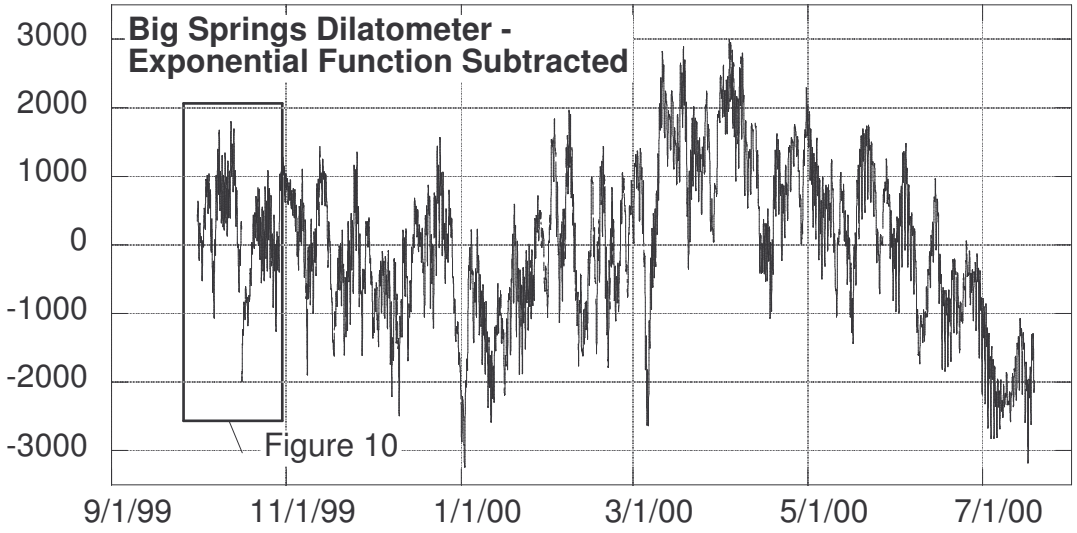

Figure 9. Big Springs dilatometer data after subtracting exponential function.

Figures 8 and 9 show data from the Long Valley Big Springs dilatometer, before and after removing an exponential trend. The exact function fit to the data is $u(t)= 0.173x10^{6} -0.843x10^{5} \exp[-0.687x10^{-2}(t)]$ where t is measured in days from the start of the useable data. The exponential function does a reasonable job of fitting the data, and after it has been removed, it's possible to discern a step-like strain change caused by the October 16, 1999 M7.1 Hector Mine earthquake, about 400 km from Long Valley (Figure 10)

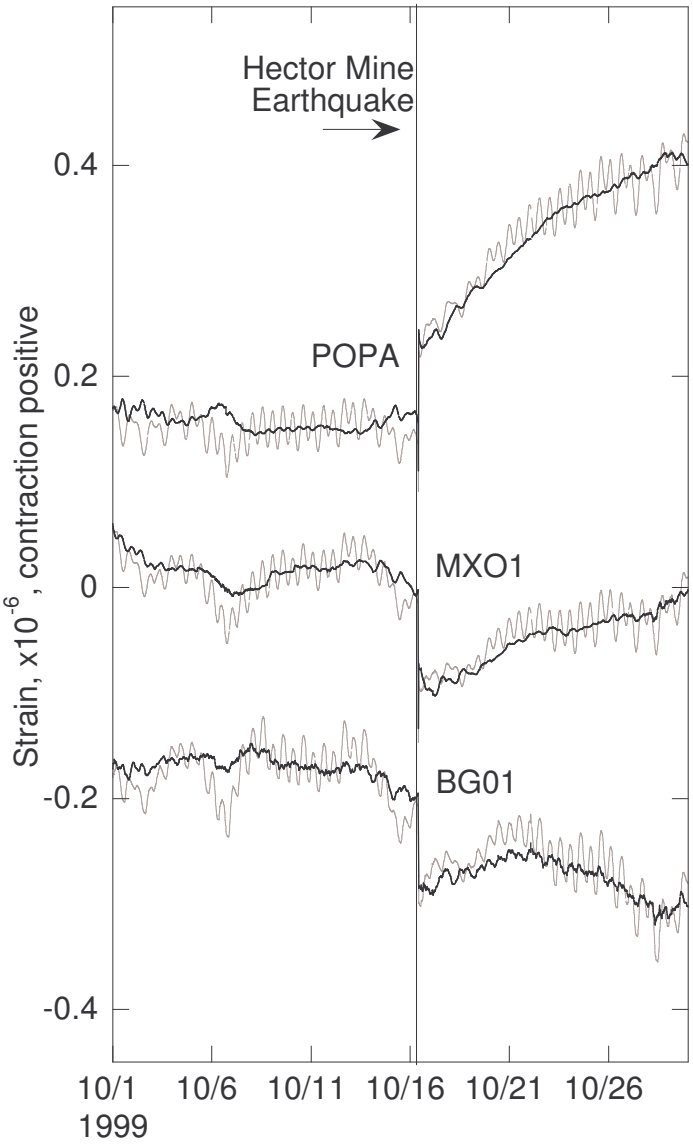

Figure 10. Data from 3 Long Valley dilatometers, after removing trends and tides

The long-term record from the San Juan Bautista (SJB) GTSM contains very large step-like strain changes caused by earthquakes and slow strain events. Figure 11 shows the raw data from the SJB 3-component borehole strainmeter for the period from 1984 until May 2005. The data shown are "raw linearized data" from the individual gages. This data set is amenable to removal of the long-term trends by fitting a sum of an exponential function, a linear function, a quadratic function, and steps of unknown size.

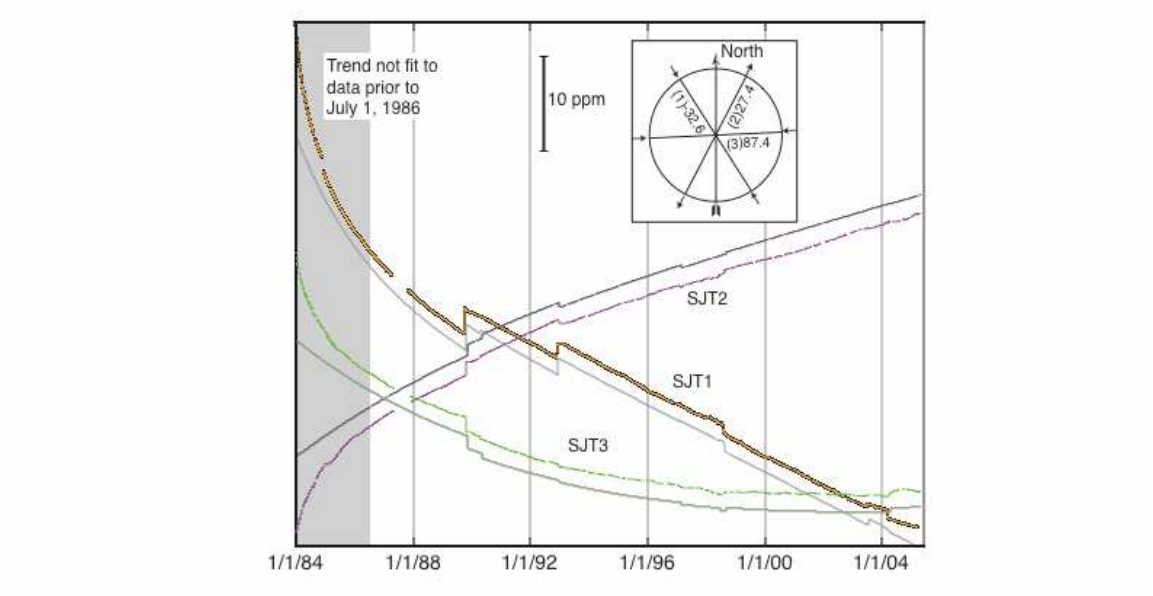

Figure 11. Raw data from the SJB 3-component borehole strainmeter for the period from 1984 until May 2005. The data shown are "raw linearized data" from the individual gages.

The data from 1984 until July 1986 are not considered because of strong post-installation trends that are interrupted by a disturbance of unknown origin, as well as by the coseismic step and postseismic rate change imposed by the M6.2 Morgan Hill earthquake on 24 April 1984, and can be shown not to fit either a quadratic or an exponential function. The additional terms in the trend function that would be required to fit this initial part of the data risks introducing spurious slope changes in the residual data. To remove the trend from the data from July 1986 on, the data on each gage were edited to remove large steps associated with earthquakes and slow slip events. Daily averages of the edited data were formed, and were fit to a function consisting of a quadratic polynomial and a decreasing exponential function, together with unknown values of strain steps occurring at the times of earthquakes and slow slip events. These functions are superimposed on the data shown in Figure 11. Figure 12 shows the original 18-minute data after subtracting these trends.

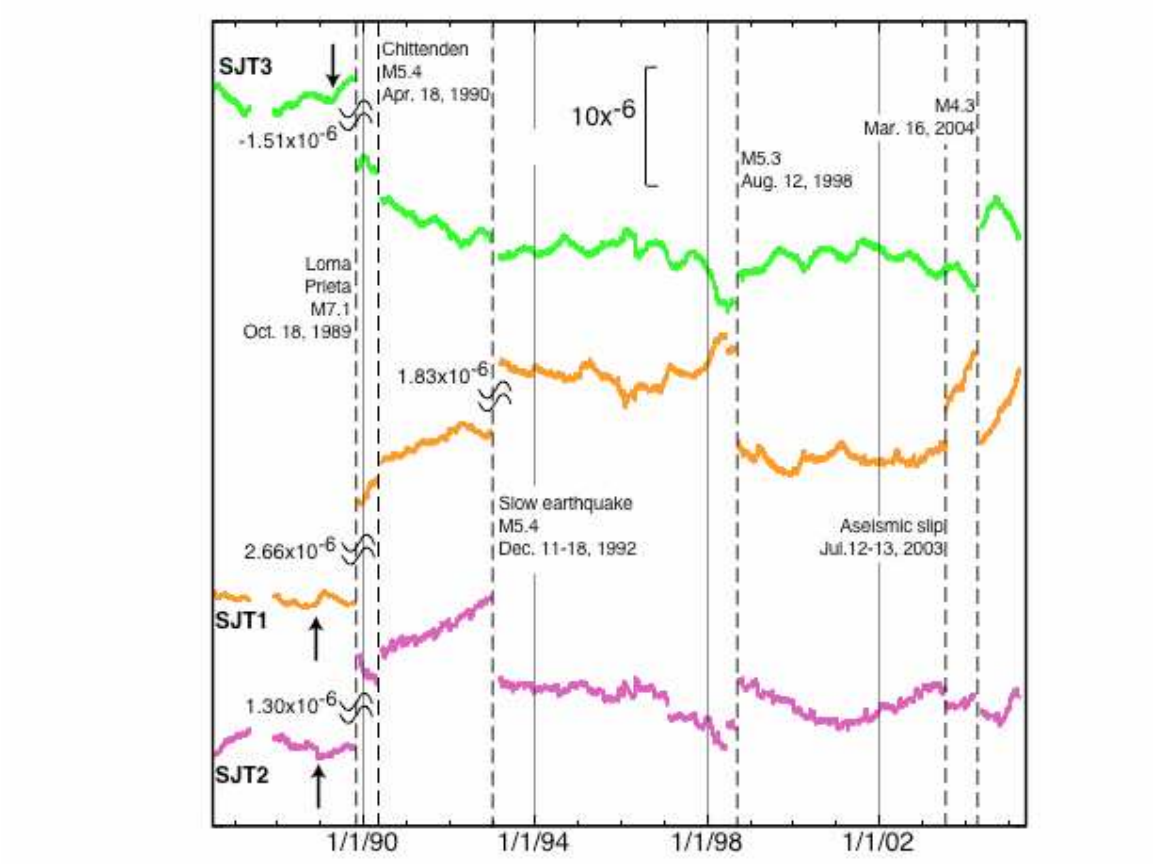

Figure 12. Original 18-minute data from SJB GTSM after subtracting the trends shown in Figure 11.

Gladwin et al. (1991) proposed that changes in shear strain rate occurred at this strainmeter prior to the 1989 M7.1 Loma Prieta earthquake. The strain rate change prior to the Loma Prieta earthquake can be seen in the data from gages 1 and 3 even without removing the strong exponential trend in the data. Gladwin et al. (1991) removed this trend by fitting two exponential functions to the much shorter data record available prior to the Loma Prieta earthquake. From Figure 12 it is evident that strain-rate changes similar to those preceding the Loma Prieta earthquake occur at many other times in the data. This does not necessarily mean that these changes were unrelated to the impending earthquake, but poses a difficulty in establishing that they are anomalous. The detrended data can be compared with the concept proposed by Gwyther et al. (2001), to the effect that this strainmeter record is approximately piecewise linear, with slope changes occurring after earthquakes and large slow strain events.

Figure 13 zooms in on the period prior to the Loma Prieta earthquake. Figure 13 shows that the rate changes prior to the Loma Prieta earthquake on gages 1 and 2 seem to initiate with abrupt steps on 21 November 1989, between 0515 and 0551 UT. These are among the list of strain events noted in Gladwin et al (1994). On gage 3, the rate change seems to begin less abruptly around April 25, 1989.

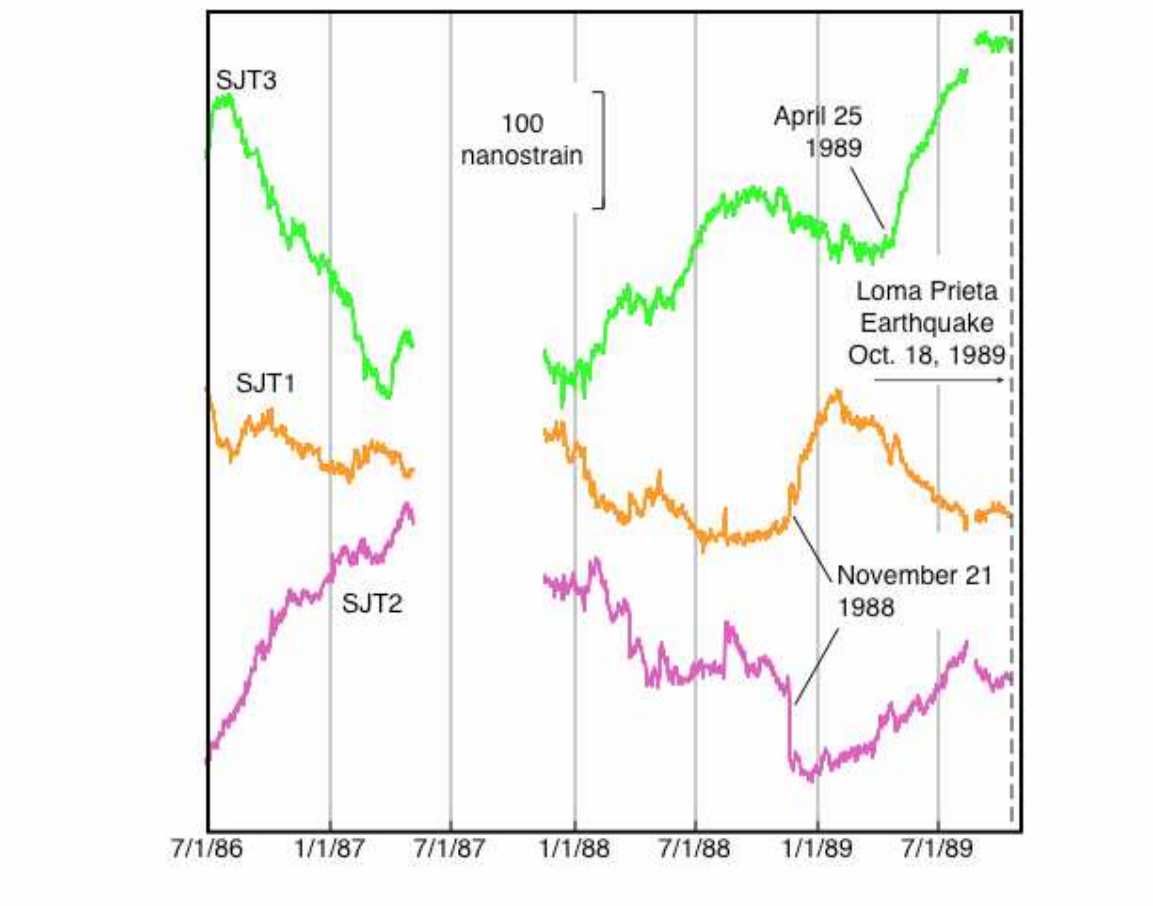

Figure 13. Original 18-minute data from SJB GTSM after subtracting the trends shown in Figure 10, for the period prior to the 1989 M7.1 Loma Prieta earthquake.

3.2 Subtracting a smooth non-parametric curve that approximates the data

A simple method for removing a long-term trend that is not easily described by a simple parametric function is to compute averages of the data at a specified interval, fit a spline curve through these points, and subtract the resulting curve from the un-averaged

data. The choice of the averaging interval provides some control over the frequency band left in the data. (Alternatively, the control points can be picked by hand and don't need to be uniformly spaced in time.) For the examples shown here, the spline interpolation is done using the Numerical Recipes subroutines dspline and dsplint.

Figures 14 through 16 illustrate this method applied to the dilatometer data from Piñon Flat. Figure 14 shows the data from the three dilatometers CIA, CIB, and CIC, which are arranged in an approximate equilateral triangle with 300 m legs. The raw data are shown, and superimposed dots are averages centered on 90-day intervals, through which a spline curve will be interpolated. The initial and final intervals may be shorter because the first and last data points are used as the first and last points to define the spline. A spline curve cannot be used for extrapolation, so if the first point defining the spline is not the first data point, then the trend cannot be computed for the beginning of the time series. Figure 15 shows the residual strain data after subtracting the spline curves interpolated through the dots. The residual data has a much smaller range and smaller features in the data can now be seen. For comparison, Figure 16 shows the same data detrended using splines fit to 180-day averages.

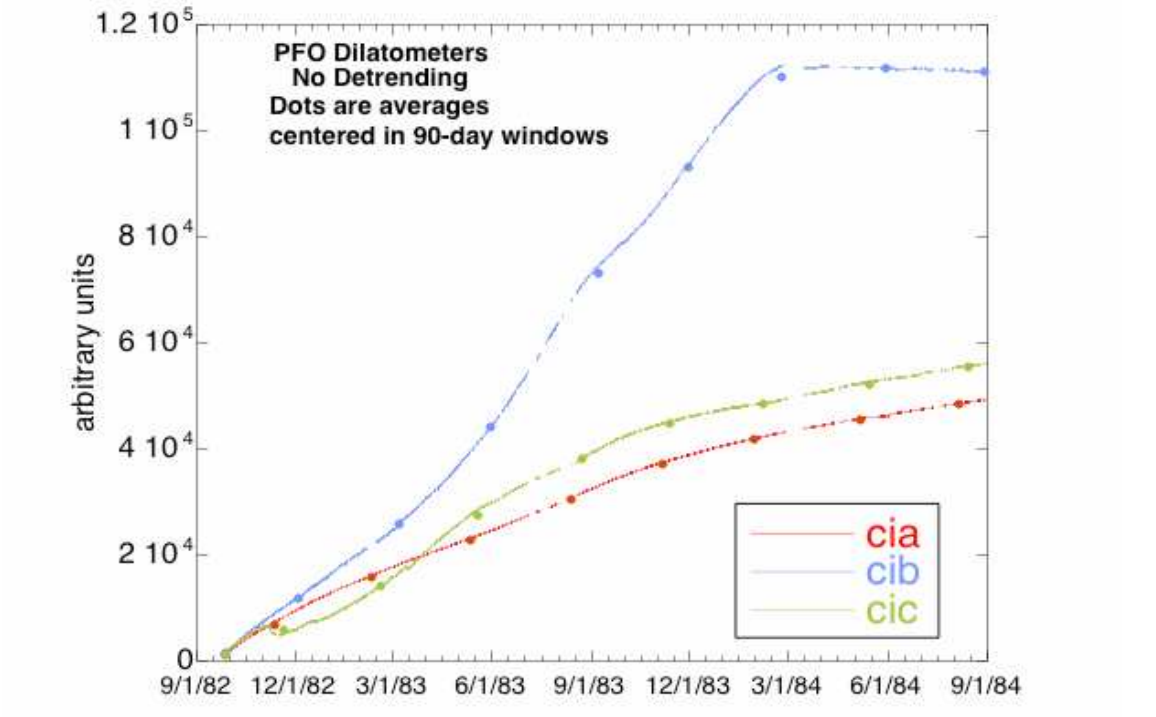

Figure 14. PFO dilatometer data with points selected for curve-fitting.

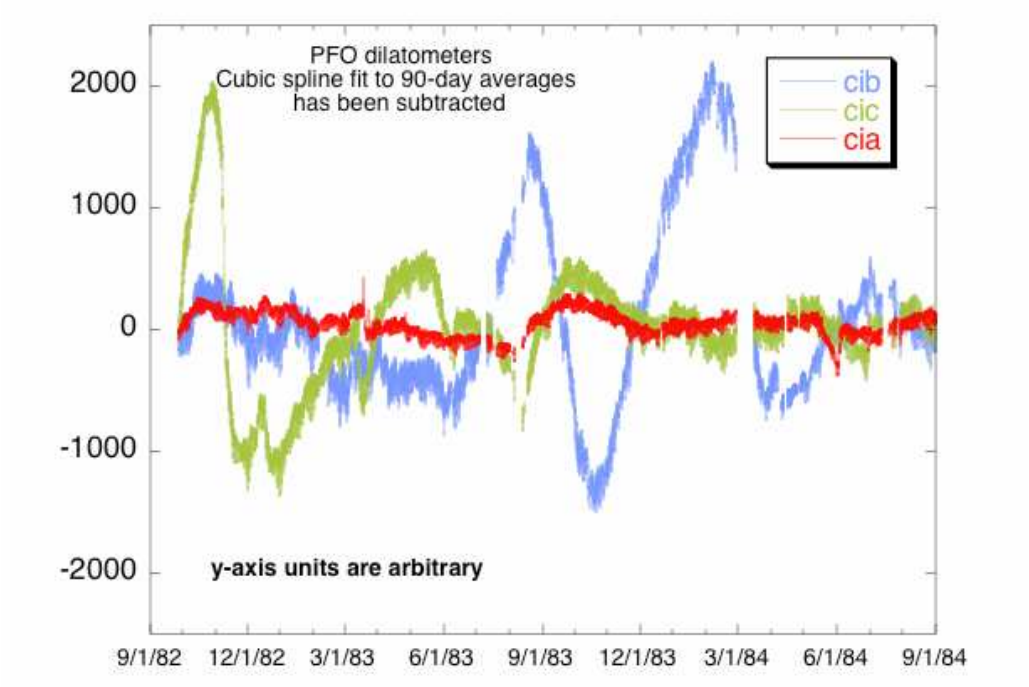

Figure 15. Residual Piñon Flat dilatometer data after subtracting the spline curves interpolated through the points shown in the previous figure.

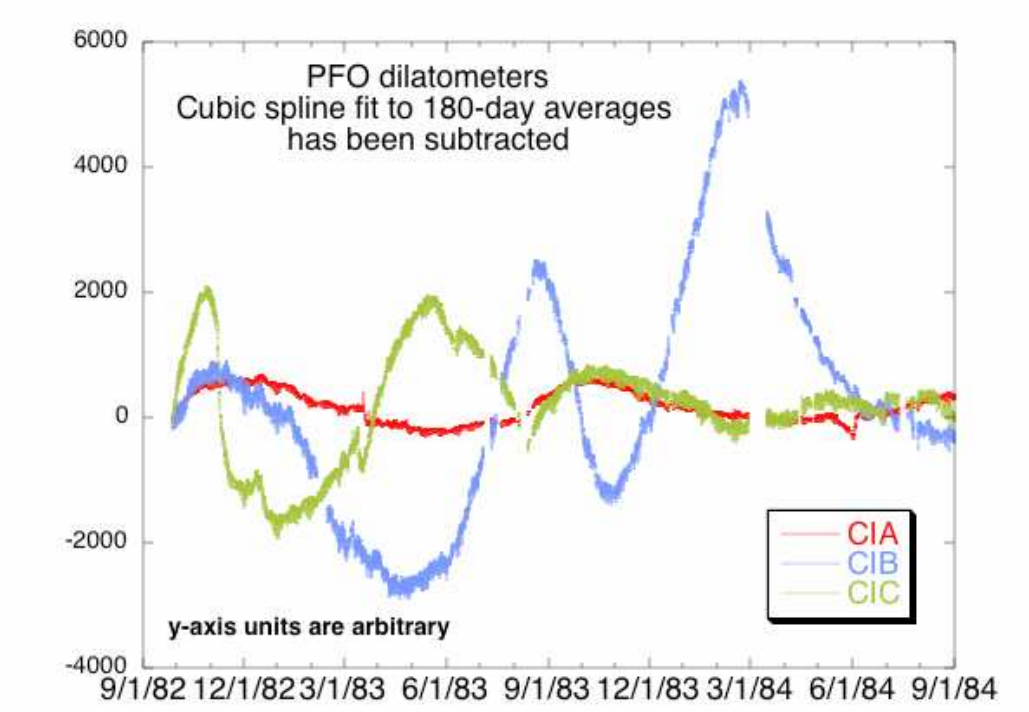

Figure 16. Same as previous figure, but residual is with respect to splines fit to 180-day averages.

It can be seen from Figure 15 that the residual strain data from the three dilatometers do not track each other in detail with respect to signals lasting from days to months. In particular, the CIB record is quite different from the records at CIA and CIC. The Piñon Flat site consists of fractured granite, and it is known that the water table is at different elevations at nearby boreholes; this type of setting may contribute to a lack of coherence between closely spaced borehole strainmeters. The first PBO borehole strainmeter installations include two clusters of three strainmeters each, within about 150 m of each other, to further investigate how well borehole strainmeters track each other at periods of days to months.

4. The Parkfield Transient: A Long-period Borehole Strainmeter Signal

Gwyther et al. (1996) first called attention to changes in the fault-parallel shear strain rates measured by two GTSM's near Parkfield, California. Beginning in 1993, the NE-striking gages of the EDT and FLT 3-component borehole strainmeters, on opposite sides of the fault (Figure 17), began recording slower extension and slower contraction, respectively, with relative rate changes of 0.1 to 0.5 x 10^{-6}/yr. Figure 18 shows these data resolved into shear strain components parallel and perpendicular to the fault. Gwyther et al. (1996) modeled the GTSM observations with upward and northwest propagation of a patch of accelerated slip centered beneath EDT (Figure 19). This strain-rate change was noticed about two years after it began, and its beginning was around the time of the first of several M>4 earthquakes near the hypocenter of the 1966 Parkfield earthquake.

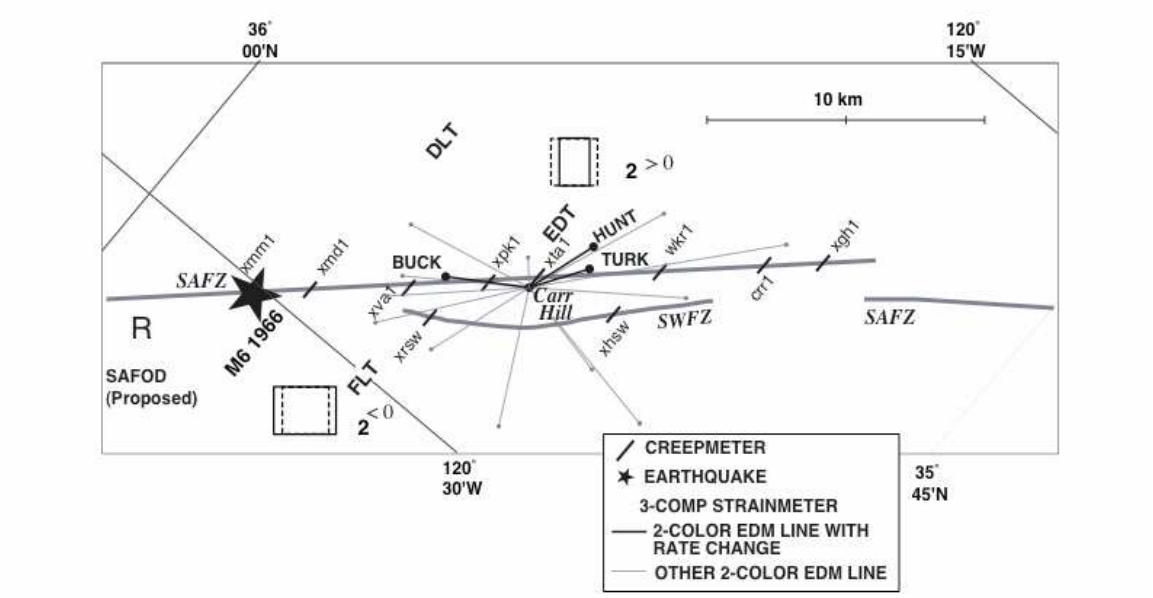

Figure 17. Map showing locations of creepmeters, the two-color EDM network, and GTSM's near Parkfield, California.

The observation was controversial for two reasons. First, the strain rate changes that appeared to have taken place 1992-1993 represent a time scale intermediate to the short periods where the GTSM works well, and steady state, where it does not work at all. The second source of controversy was the coincidence of the strain rate change with an increase in annual rainfall. The cumulative annual precipitation could also be viewed as having a rate change between 1993 and 1995 (Figure 8+N+8).

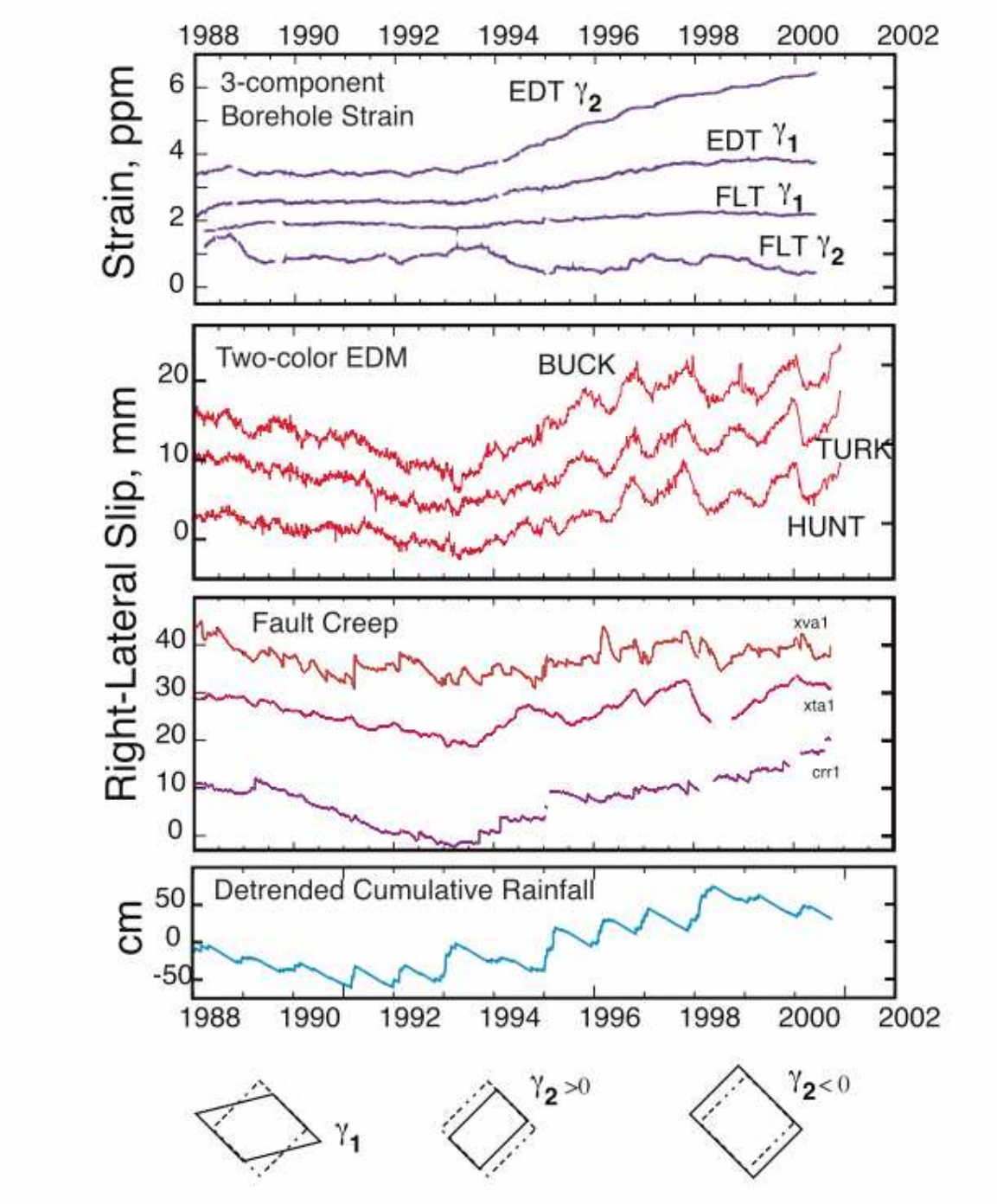

Figure 18. Data from Parkfield GTSM's 2-color EDM, and creepmeters.

The idea that the rate changes could be local to the GTSM's was disproven when measurements made by the two-color EDM network revealed that three fault-crossing, near fault-parallel baselines had begun to lengthen or shorten more rapidly since early 1993. Langbein et al. (1999) modeled the combined GTSM and EDM data sets using a

spatially smooth slip rate distribution. This slip rate distribution places the area of greatest slip acceleration to the northwest of EDT and FLT, extending to a depth of at least 5 km, with acceleration of fault slip by as much as 8 mm/year. A shallower area of increased slip rate is inferred beneath the EDM network at Carr Hill. A similar result was obtained by Gao et al. (2000). Faster relative slip since 1993 was also indicated by several creepmeters (CRR1, XTA1, and XVA1) in Parkfield. Roeloffs et al. (2001) examined the Parkfield creep dataset to determine which instruments characteristically respond to rainfall, and to correct for seasonal variations at several sites. She judged a creep rate increase at CRR1 most likely to be tectonic because it includes discrete steps unrelated to rainfall, and because CRR1 has not exhibited accelerated creep in response to rainfall in the past. Like the creepmeters, the EDM network utilizes surface monuments that could be destabilized by rainfall.

Nadeau et al. (1999) developed a method for inferring fault slip rate from the average recurrence interval in each cluster of repeating Parkfield microearthquakes, and showed that the M>4 seismicity during 1992-1994 was accompanied by a rather widespread decrease in these recurrence intervals. Figure 19 superimposes the total area of the fault for which Nadeau et al. (1999) inferred slip rate increases of 5 mm/year or more on the areas of accelerated slip inferred from the EDM and BTSM data. All studies find a zone of greatly increased slip rate on the fault section north of FLT. Beneath Carr Hill, however, the microearthquake recurrence intervals show shortening only in the depth range 7 to 12 km, while the EDM data, and to some extent the creep data, indicate accelerated slip at shallower depths.

Since 1997, there is some indication in the 2-color EDM and GTSM data that the rate changes have changed character or returned to their pre-1993 rates (J. Langbein, personal communication).

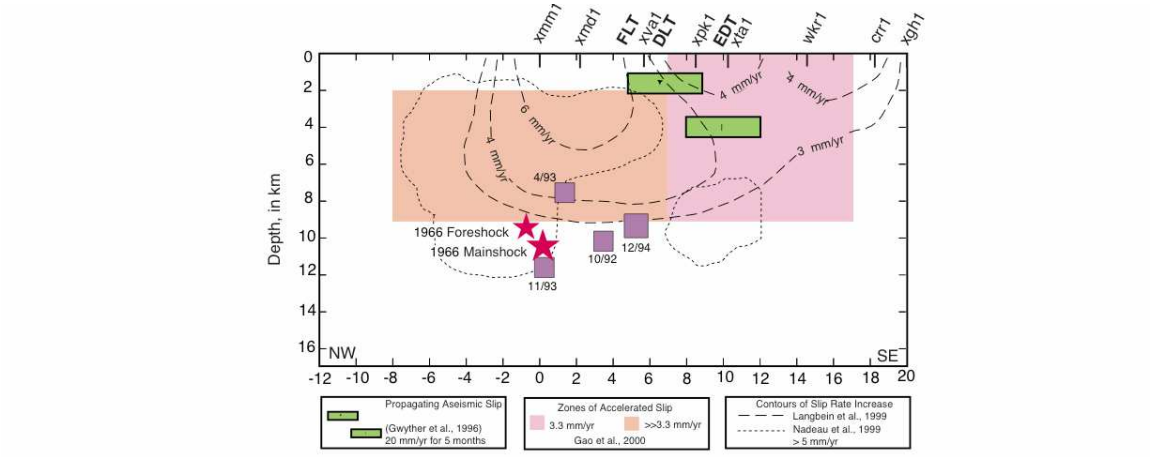

Figure 19. Cross-sectional diagram showing inferred locations of accelerated aseismic fault slip beginning in 1993 on the San Andreas fault near Parkfield.

These slip-rate variations, although not greatly above the detection limit of the Parkfield instrumentation, constitute a very sizeable change in the aseismic deformation rate along the San Andreas fault. The γ_2 shear strain rate can be viewed as a measurement of slip rate change along the strike of the fault. Surface creep rate at Parkfield varies approximately linearly with distance, decreasing from 15 mm/yr to zero from NW to SE over the 34 km-long segment. This creep-rate gradient corresponds to a roughly uniform fault-parallel shear strain rate of +/- 0.22 x 10^{-6}/yr, assuming the strain is divided equally between the two sides of the fault . γ_2 is positive on the NE side of the fault, and negative on the SW side. Thus the observed GTSM rate changes of 0.5 to 0.6 x 10^{-6}/yr represent accelerations of the background strain rates that amount to an approximate doubling of the along-fault slip gradient, at least locally near FLT and EDT. Inferred subsurface slip-rate changes of 5 mm/yr or more represent increases of at least 25% of the background rate.

The GTSM signals documenting the "Parkfield transient", as it has come to be called, could be evaluated because the creepmeters and 2-color EDM were also able to record the increased slip rate. However, creepmeters cannot be used in most settings, and the 2-color EDM is an aging prototype instrument that is being retired. Continuous GPS would probably not have been sensitive enough to discern the increased slip rate.

5. Cross-spectral analysis to evaluate long-period response

If a known strain signal with energy at long periods were available, then examining the relationship between the strainmeter data and the known signal as a function of frequency would be a way to learn how the strainmeter responds at long periods. Volumetric strain changes in response to atmospheric pressure variations provide a known signal with energy at periods of a few tens of days. (Actually, atmospheric pressure variations have a strong annual component, but many of the barometers installed at California strainmeter sites are not stable enough to record these accurately.) For any known signal, the cross-spectrum can be used to estimate how strainmeter response varies as a function of frequency.

5.1 Estimating transfer functions using the cross-spectrum

In the time domain, consider the strainmeter response, $y(t)$, to atmospheric pressure, $x(t)$, as a single-input, single-output linear system, ie.,

$$y(t) = \int_0^\infty h(u)x(t-u)du \qquad (1)$$

where $h(u)$ is a weighting function that gives the impulse response of the system. The Fourier transform of $h(u)$ is a function of frequency, $H(\omega)$, called the transfer function or frequency response function. We would like to know if this transfer function varies with frequency, so we use the cross-spectrum to estimate the transfer function from the strain and atmospheric pressure data. Included here is an outline of this technique; for proofs, rigor, and details see Chapter 9 of Chatfield (1996) and in Chapter 6 of Bendat and Piersol (1986).

Taking the Fourier transform of both sides of (1) yields the relationship

$$Y(\omega) = H(\omega)X(\omega) \qquad (2)$$

where $Y(\omega)$ and $X(\omega)$ are the Fourier transforms of the strain data and the atmospheric pressure data. In general, $H(\omega)$, $X(\omega)$, and $Y(\omega)$ are complex and it is useful to think of them as having amplitudes and phases.

Although it is straightforward to compute $X(\omega)$ and $Y(\omega)$ from the data, in the presence of noise, equation (2) does not provide a practical means of estimating $H(\omega)$. Instead, make equation (1) more realistic by adding a noise term, $N(t)$, so that

$$y(t) = \int_0^\infty h(u)x(t-u)d\tau + N(t). \quad (3)$$

It is assumed that $N(t)$ and $x(t)$ are uncorrelated, ie., that

$$\int_0^\infty x(t-\tau)N(\tau)d\tau = 0 \quad (4)$$

Multiply both sides of equation (3) by $x(t-\tau)$ and integrate from 0 to ∞, and use equation (4), to obtain:

$$g_{xy}(\tau) = \int_0^\infty h(u)g_{xx}(\tau - u)du \quad (5)$$

where

$$g_{xx}(\tau) = \int_0^\infty x(u)x(\tau - u)du \quad (6a)$$

$$g_{xy}(\tau) = \int_0^\infty x(u)y(\tau - u)du \quad (6b)$$

are the auto-covariance of the input and the cross-covariance of the input and output, respectively. Finally, take Fourier transforms of both sides of equation (5) to obtain

$$G_{xy}(\omega) = H(\omega)G_{xx}(\omega) \quad (7)$$

in which $G_{xy}(\omega)$ is the cross-spectrum of the input and output, and $G_{xx}(\omega)$ is the autospectrum of the input. The (complex) transfer function can be estimated from (7) as

$$H(\omega) = G_{xy}(\omega)/G_{xx}(\omega). \quad (8)$$

The transfer function is best thought of as having a gain, $|H(\omega)|$, and a phase shift, $Arg[H(\omega)]$.

The cross-spectrum and autospectrum are defined as the Fourier transforms of the cross-covariance and auto-covariance, respectively. However, instead of computing them this way in practice, a different method is used based on Fourier transforms of the data taken over finite intervals. For input and output functions that are measured over a finite time interval, T, it can be shown that

$$G_{xy}(\omega) = 2\lim_{t->\infty}\{\frac{1}{T}E[X_k^*(\omega,T)Y_k(\omega,T)]\} \quad (9a)$$

$$G_{xx}(\omega) = 2\lim_{t->\infty}\{\frac{1}{T}E[|X_k(\omega,T)|^2]\} \quad (9b)$$

$$G_{yy}(\omega) = 2\lim_{t->\infty}\{\frac{1}{T}E[|Y_k(\omega,T)|^2]\} \quad (9c)$$

in which $E[...]$ denotes taking the expectation. The equivalence of equations (9a) through

(9c) to the original definitions of the auto- and cross- spectra is proved in section 9.2.2 of Bendat and Piersol (1986). In applying these equations to real data, the limiting process is ignored, and the process of taking the expectation amounts to averaging over spectra computed from subsets of the data. Note that (9b) and (9c) are the power spectra of the input and output, respectively.

Another useful quantity is the coherence, defined as

$$coh_{xy}^2(\omega) = \frac{\left|G_{xy}(\omega)\right|^2}{G_{xx}(\omega)G_{yy}(\omega)} \qquad (10)$$

It can be shown that $coh_{xy}^2(\omega)$ is a number between 0 and 1, and it is a measure of how well correlated the output is with the input, with 1 indicating perfect correlation. More specifically, if $coh_{xy}^2(\omega)$ is smaller than 1, then either there is "extraneous noise" in the system, the system is nonlinear, or there is some other input that has not been taken into account (Bendat and Piersol, 1986).

The ideas in equations (1) through (10) were developed for engineering control applications, where very good estimates of spectra can be obtained because the input and output signals can be measured hundreds or thousands of times. A borehole strainmeter record is inherently an unrepeatable experiment. If we are using 6-month long records of strainmeter data that overlap by 3 months, and we have 10 years of data, that's only 40 spectra that are available for ensemble averaging. The consequence of this reality is that the coherence standards for studying strain data are far more relaxed than those recommended in texts on engineering applications.

Below we discuss transfer functions between dilatometer data and atmospheric pressure. An earlier example of the use of this technique to study response of groundwater levels to atmospheric pressure is given in Quilty and Roeloffs (1991).

5.2 Atmospheric Pressure Response for Dilatometers.

The frequency dependence of the response to atmospheric pressure was estimated using cross-spectral analysis for several California dilatometers, primarily as a way of investigating the performance of the instruments at periods longer than 1-2 days. In order to have enough spectra of individual records to average together, most spectra were

computed using 6-month sections of the data, overlapping where possible. Data were detrended by subtracting spline functions fit to 180-day averages of the data; this removes signals with periods of about 6 months or longer, so the transfer function estimates are not meaningful for longer periods. It was of particular interest to examine the frequency-dependent responses of instruments suspected of not tracking strain over periods much longer than tidal periods.

Figures 20a,b show the gain and coherence of volumetric strain with respect to atmospheric pressure for the Parkfield Jack Canyon dilatometer. This instrument has a long data record and one of the best signal-to-noise ratios in the tidal band in the Parkfield area. The coherence is above 0.6 for periods as long as 62 days and the response is flat to at least this long a period. At neither site is there obvious evidence of a falloff in response to atmospheric pressure down to the lowest frequencies evaluated, although gain values with low corresponding coherences may not be meaningful.

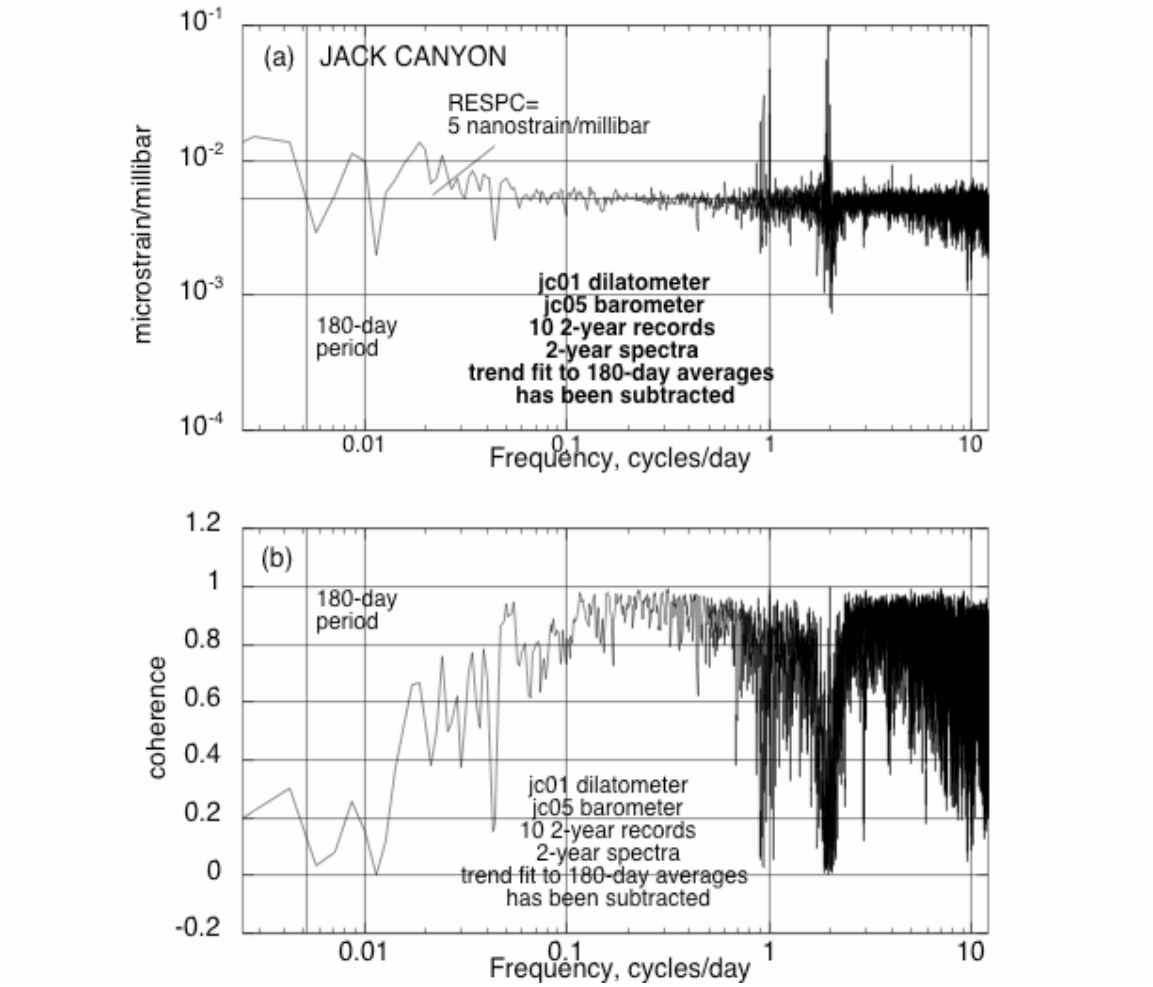

Figure 20. (a) Gain of estimated transfer function between Jack Canyon dilatometer and atmospheric pressure. (b) Coherence.

The Red Hills dilatometer response is shown in Figures 21a,b. The coseismic step at this site due to the 22 December 2003 San Simeon earthquake recovered in about 1 day, suggesting that the Red Hills instrument may not be well coupled to the crust at these periods. However, the response to atmospheric pressure is flat for periods as long as 60 days.

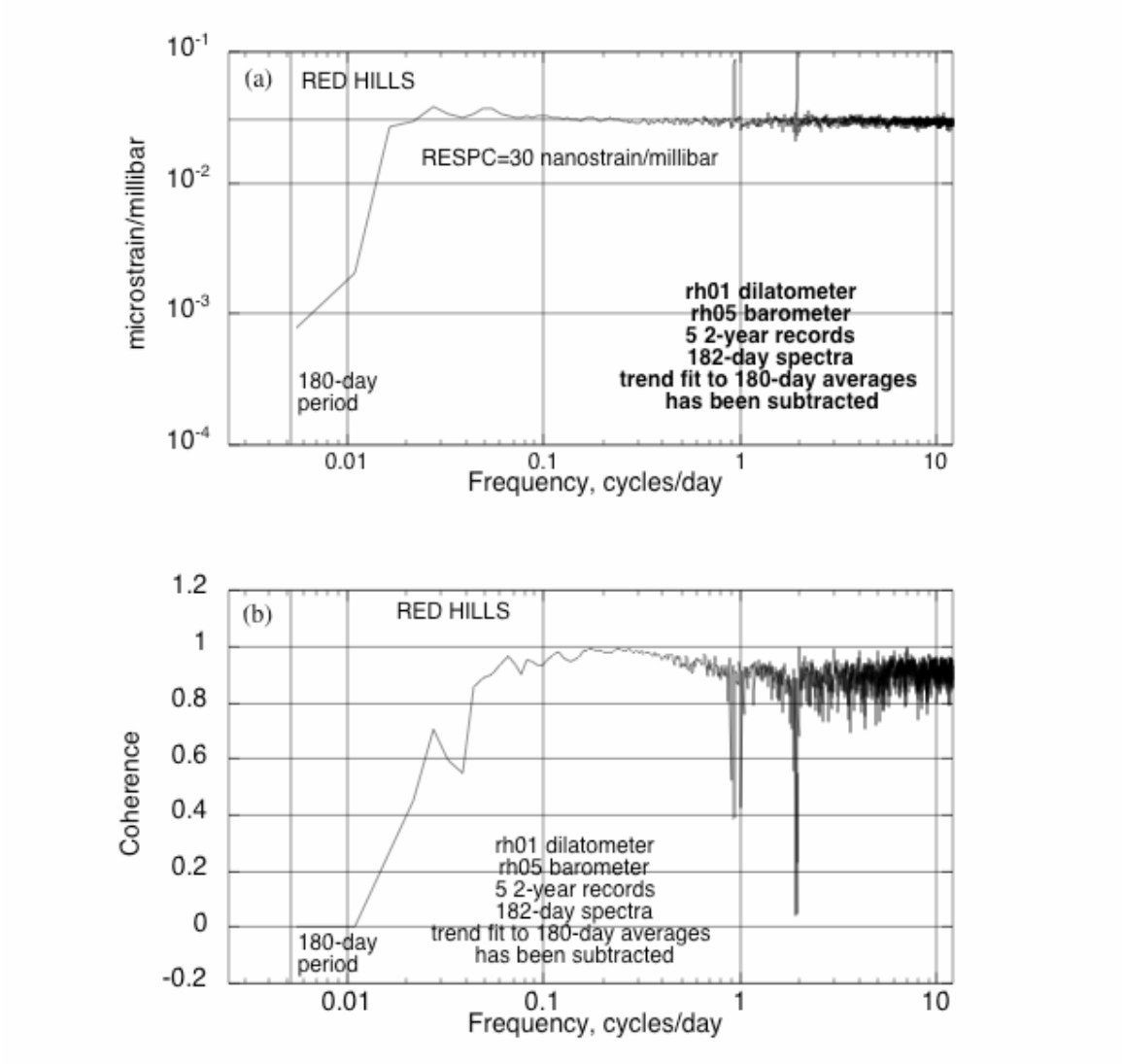

Figure 21. Gain of estimated transfer function between Red Hills dilatometer and atmospheric pressure. (b) Coherence.

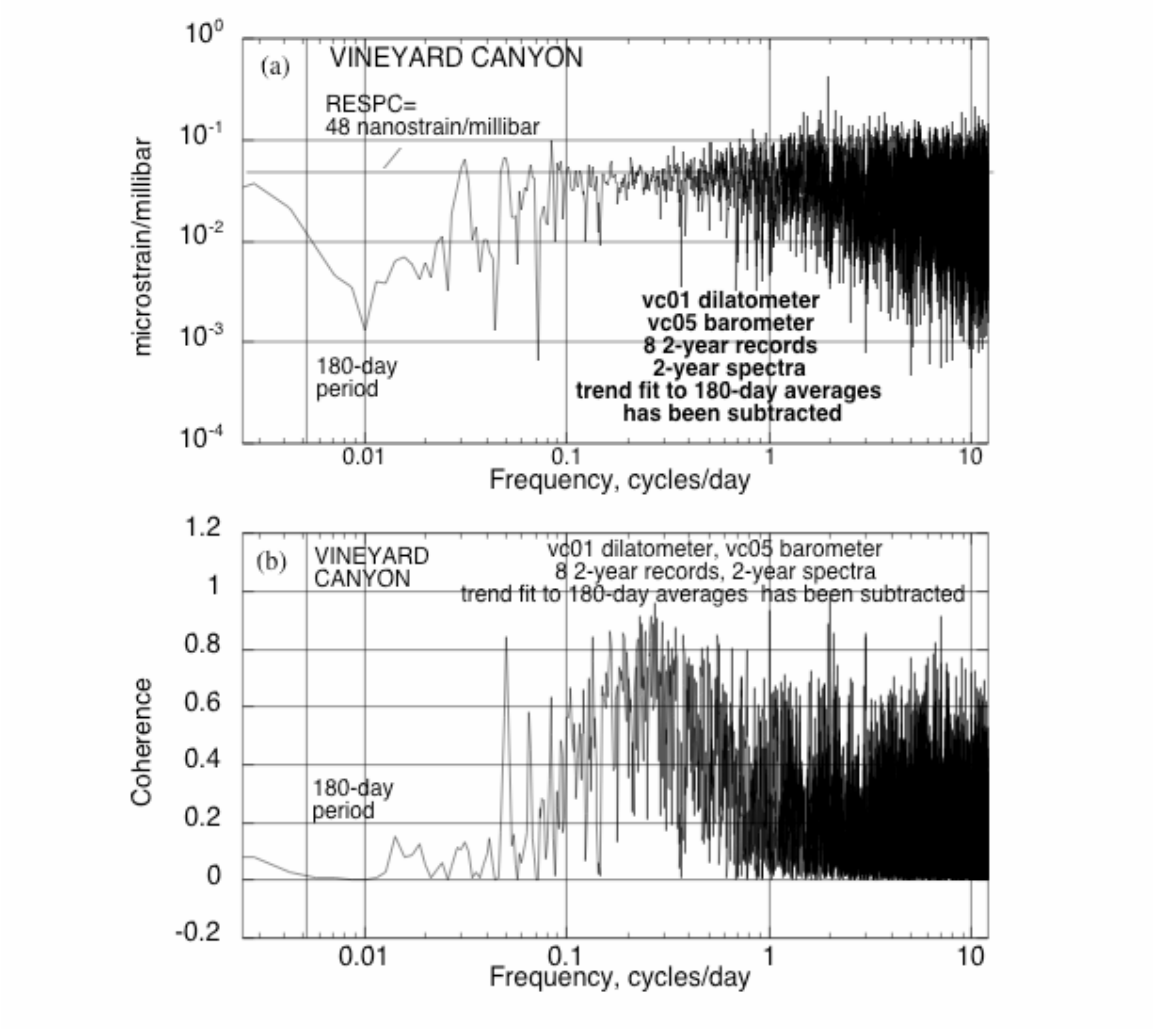

Figure 22. Gain of estimated transfer function between Vineyard Canyon dilatometer and atmospheric pressure. (b) Coherence.

The Vineyard Canyon dilatometer response is shown in Figure 22a,b. The long-term strain at this site is extensional (Figure 1), which might be taken as evidence of poor coupling to the crust outside the borehole. For this site, the atmospheric pressure response does fall with increasing period for periods longer than 10 days.

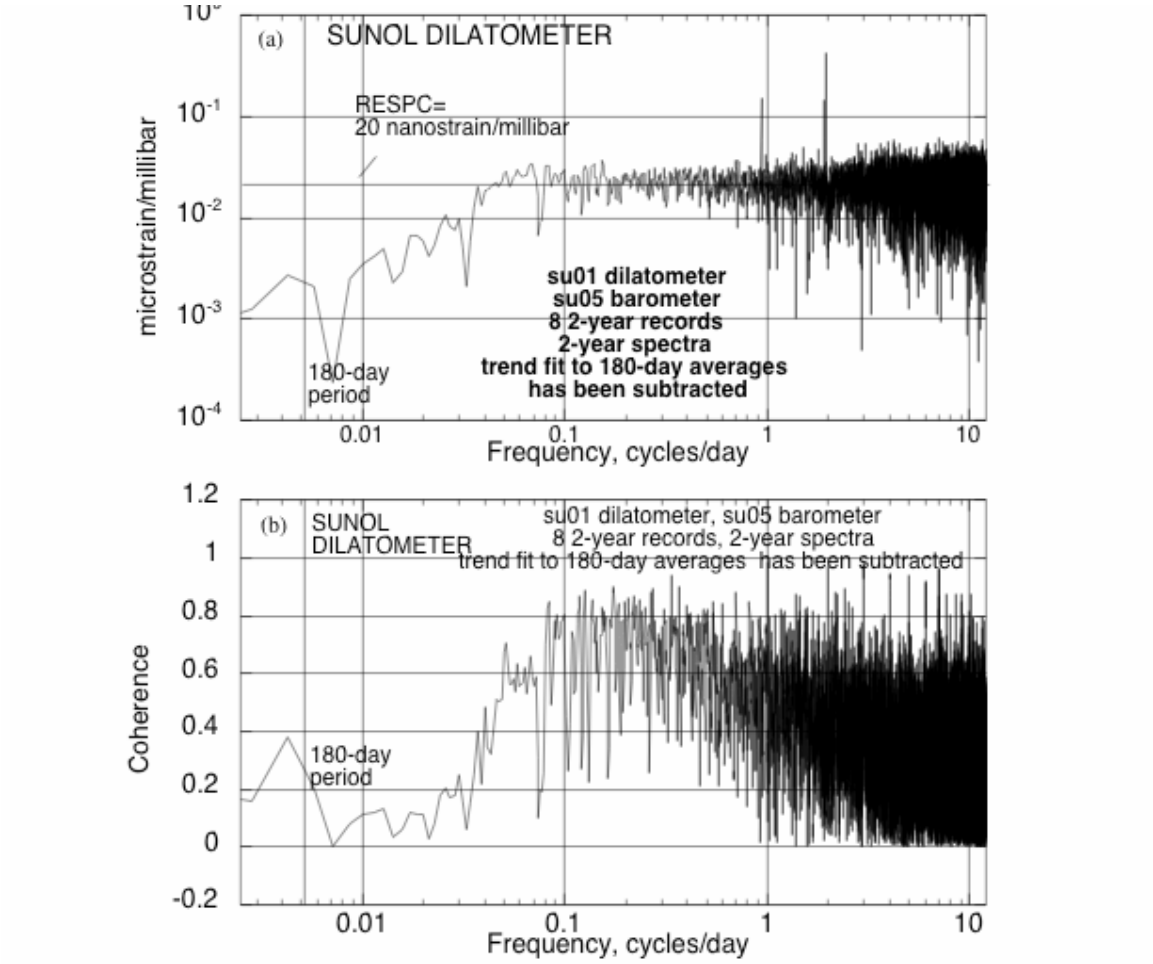

Figure 23. Gain of estimated transfer function between Sunol dilatometer and atmospheric pressure. (b) Coherence.

The Sunol dilatometer in the east San Francisco Bay area is another dilatometer with a long-term extensional trend. Its response to atmospheric pressure is shown in Figures 23a,b. The Sunol dilatometer also exhibits a decrease of gain for periods longer than 40 days.

The conclusion from the frequency-dependent atmospheric pressure responses that were computed is that the two dilatometers with extensional long-term trends also exhibit decreases in the gain of the atmospheric pressure response for periods longer than 10 and 40 days, respectively. The response to tectonic strain at these two instruments can also be expected to decrease for periods longer than these values. In these two cases, and perhaps generally, the lack of a long-term contractional strain seems to be evidence of poor long-term coupling to tectonic strain.

Literature Cited

Bendat JS, Pierson AG. 1986. Random data. 2nd Edition. John Wiley and Sons, 566 pp.

Chatfield C. 1996. The Analysis of Time Series: An Introduction. Fifth Ed., Chapman & Hall, London, 283 pp.

Gao, S., Silver, P.G. & Linde, A.T. 2000. Analysis of deformation data at Parkfield, California: Detection of a long-term strain transient. *J. Geophys. Res.* **105**:2955-67.

Gladwin MT, Gwyther RL, Higbie JW, Hart RHG. 1991. A medium term precursor to the Loma Prieta earthquake? *Geophys. Res. Lett.* 18:1377-80.

Gladwin MT, Gwyther RL, Hart RHG, Breckenridge KS. 1994. Measurements of the strain field associated with episodic creep events on the San Andreas fault at San Juan Bautista, California. *J. Geophys. Res.* 99:4559-65.

Gwyther RL, Gladwin MT, Mee M, Hart RHG. 1996. Anomalous tensor strain at Parkfield during 1993-1994. *Geophys. Res. Lett.* 23:2425-28.

Gwyther, R. L., Gladwin, M. T.,Hart, R., Mee, M. 2001. Aseismic stress transfer between shallow and medium depths in transition zones of the San Andreas fault. American Geophysical Union, Fall Meeting 2001, abstract #S22A-0616.

Hodgkinson, K. 2004. Review of borehole tiltmeter data collected by the U.S. Geological Survey. UNAVCO report, 43 pages. Available from:

Langbein JO, Gwyther RL, Hart RHG, Gladwin MT. 1999. Slip rate increase at Parkfield in 1993 detected by high-precision EDM and borehole tensor strainmeters. *Geophys. Res. Lett.* 26:2529-32.

Nadeau, R.M. & McEvilly, T.V. 1999. Fault slip rates at depth from recurrence intervals of repeating microearthquakes. *Science* **285:**718-721.

Quilty E, Roeloffs E. 1991. Removal of barometric pressure response from water level data. J. Geophys. Res. 96:10,209-10,218.

Roeloffs, E. 2001. Creep-rate changes at Parkfield, California 1966-1999: Seasonal, precipitation-induced, and tectonic. J. Geophys. Res. 106:16525-47.

Online Resource

Numerical Recipes Home Page
http://www.nr.com/